Journal of Sound and Vibration 329 (2010) 3304–3318

Contents lists available at ScienceDirect

Journal of Sound and Vibration

journal homepage: www.elsevier.com/locate/jsvi

Analysis of wave propagation in a thin composite cylinder with periodic axial and ring stiffeners using periodic structure theory

Sungmin Lee [a,*], Nickolas Vlahopoulos [b], Anthony M. Waas [c]

[a] Department of Mechanical Engineering, University of Michigan, Ann Arbor, MI 48109-2125, USA
[b] Department of Naval Architecture and Marine Engineering/Mechanical Engineering, University of Michigan, Ann Arbor, MI 48109-2145, USA
[c] Department of Aerospace Engineering/Mechanical Engineering, University of Michigan, Ann Arbor, MI 48109-2140, USA

ARTICLE INFO

Article history:
Received 14 May 2009
Received in revised form
22 December 2009
Accepted 23 February 2010
Handling Editor: D. Juve
Available online 25 March 2010

ABSTRACT

Wave propagation characteristics of a thin composite cylinder stiffened by periodically spaced ring frames and axial stringers are investigated by an analytical method using periodic structure theory. It is used for calculating propagation constants in axial and circumferential directions of the cylindrical shell subject to a given circumferential mode or axial half-wave number. The propagation constants corresponding to several different circumferential modes and/or half-wave numbers are combined to determine the vibrational energy ratios between adjacent basic structural elements of the two-dimensional periodic structure. Vibration analyses to validate the theoretical development have been carried out on sufficiently detailed finite element model of the same dimension and configuration as the stiffened cylinder and very good agreement is obtained between the analytical and the dense finite element results. The effects of shell material properties and the length of each periodic element on the wave propagation characteristics are also examined based on the current analytical approach.

1. Introduction

It is often found that an airplane or a rotorcraft fuselage consists of thin composite cylindrical shells with orthogonal stiffeners which are usually spaced at quite regular intervals in both the axial and circumferential directions. These structures are often considered to be spatially periodic in order to evaluate their dynamic properties. The spatial periodicity allows elastic waves to propagate in certain frequency ranges and does not permit wave propagation in other frequency ranges and these pass/stop bands are unique characteristic of periodic structures [1–3].

Free and forced wave motions through periodically-stiffened cylinders have been studied extensively. Mead [4] has summarized a collection of state-of-the-art analytical and numerical wave-based methods among which two effective and widely used methods are mentioned herein.

First, the transfer matrix method in conjunction with periodic structure theory was applied by Mead and Bardell [5,6] to the free wave propagation in an isotropic circular cylinder with periodic axial and circumferential stiffeners. In their work, a two-dimensional periodic cylinder was reduced for analytical purposes to two separate one dimensional stiffened cylinders by assuming simply-supported boundary conditions either at ring frames or at axial stiffeners, and the pass/stop bands were identified in terms of propagation constants for each axial or circumferential mode number. Later, they also

* Corresponding author. Tel.: +1 734 846 5027.
E-mail address: ohbang@umich.edu (S. Lee).

0022-460X/$ - see front matter © 2010 Elsevier Ltd. All rights reserved.
doi:10.1016/j.jsv.2010.02.023

used the hierarchical finite element method to find the propagation frequencies of elastic waves by computing phase constant surfaces for a number of different cylinder-stiffener configurations [7,8].

A different wave-based approach called space-harmonic method has also been employed due to its effectiveness in the analysis of sound radiation from a vibrating periodic structure [4]. Hodges et al. [9] used the method to find the low order natural frequencies and modes of a ring-stiffened cylindrical shell. Since then, many researchers [10–12] have adopted the method of space harmonics to analyze the vibro-acoustic interactions of a periodic structure and fluid. For example, Yan et al. [12] analyzed the vibro-acoustic power flow of an infinite fluid-filled isotropic cylindrical shell with periodic stiffeners.

Although the aforementioned analytical methods are focused on quasi-one dimensional wave propagation problems where vibrational energy flows in one direction (e.g., along the length) with wave motion in the other direction (e.g., around the circumference) assumed to be spatially harmonic, they may be effectively utilized to compute the wave power transmission in two dimensional periodic cylinders. For example, Wang et al. [13] used the transfer matrix method based on periodic structure theory to calculate transferred vibrational energy level in aircraft-like aluminum cylinder with periodic axial and circumferential stiffeners and obtained a good agreement with experimental data (see also Ref. [14]). The same method was also applied for the high frequency vibration analysis of cylindrical shells with periodic circumferential stiffeners immersed into heavy fluid and subjected to axisymmetric excitation. The corresponding results agreed well with a very fine axisymmetric structural-acoustic finite element model [15].

All of the previous developments, however, are restricted to cylinders made only of isotropic materials. These techniques need to be extended for the wave propagation analysis of periodic composite laminate cylindrical structures of interest to many engineering applications. Among recent works associated with the vibration analysis of composite cylinders with discrete stiffeners, Zhao et al. [16] analyzed simply supported rotating cross-ply laminated cylindrical shells with different combination of axial and circumferential stiffeners. The effects of the stiffeners on the natural frequencies of the structure were evaluated via a variational formulation with individual stiffeners treated as discrete elements. More recently, Wang and Lin [17] presented an analytical method to obtain the modal frequencies and mode shape functions of ring-stiffened symmetric cross-ply laminated cylindrical shells. Both publications presented the formulation of governing equations for the vibration analysis of composite cylinders with periodic stiffeners based on either dynamic equations of motion or variational principle. Neither of the two publications addresses the evaluation of the wave propagation constants between adjacent periodic units using periodic structure theory.

Hence this paper aims to fill this specific void in the wave propagation analysis by combining periodic structure theory with classical lamination theory. The latter is more than adequate for the present study since the ratio of the cylinder radius to the thickness tends to be of the order of 500 and greater in many aircraft and rotorcraft fuselage applications of interest. Furthermore, if the wave energy ratios between two adjacent periodic elements are of primary interest, Mead and Bardell's wave-based approach provides the technical foundation that can be extended to composite cylinders. In this development, two eigenvalue problems for longitudinal and circumferential wave propagations are formulated in terms of elastic constants of composite laminates and the attenuation constants (the real part of propagation constants) are calculated for each circumferential mode number or axial half-wave number. After evaluating the wave attenuation constants, the energy ratio between two adjacent periodic elements is also computed. Thus, the analytical method presented in this paper can be used for computing the wave propagation constants and the energy ratio between adjacent periodic units of a composite laminated cylinder with metallic axial and ring stiffeners.

For the validation of this analytical method, the computed attenuation constants and/or energy ratios of a periodic composite structure are compared to those from the vibration analysis of very dense finite element models, which are regarded as quasi-exact solutions. Based on the current analytical approach, the effects of shell material properties and the periodic element length on the transferred wave energy from one periodic element to the next have been investigated in detail.

2. Periodic structure theory

When a harmonic wave with wavenumber k propagates along a periodic structure of infinite length in one-dimension, there is a phase difference kl between the wave motions at corresponding points in any pair of adjacent units with a length of l. In addition, the elastic wave motion over the distance l from one bay to the other may have the logarithmic decay rate of δl which is zero for propagating waves and nonzero for evanescent waves in undamped periodic structures. The phase difference and logarithmic decay rate are combined to have a complex propagation constant $\mu(=\delta+ik)$ so that edge displacements and the associated forces at one point in the jth element ($\mathbf{d}_L^j$ and $\mathbf{F}_L^j$, say) are related to those at the corresponding point in the adjacent $(j+1)$th element ($\mathbf{d}_L^{j+1}$ and $\mathbf{F}_L^{j+1}$, say) as follows:

$$\begin{Bmatrix} \mathbf{d}_L^j \\ \mathbf{F}_L^j \end{Bmatrix} = e^{\mu} \begin{Bmatrix} \mathbf{d}_L^{j+1} \\ \mathbf{F}_L^{j+1} \end{Bmatrix} \tag{1}$$

where superscripts stand for the periodic element number and subscripts represent the specific location (left edge for this case) of the point in the element. Furthermore, the directions of displacements and forces are assumed to be collinear with the wave propagation direction. This transformation property of traveling waves in a periodic system is well known as

Bloch's or Floquet's theorem [18]. Note here that the attenuation constant, the real part of the propagation constant, δ, represents the decay rate in the wave motion over the length of one bay in the wave propagation direction and the phase constant, the imaginary part, k, represents the phase change over the same length.

Since the continuity of displacements and tractions at the junction between the adjacent two bays requires

$$\begin{Bmatrix} \mathbf{d}_L^{j+1} \\ \mathbf{F}_L^{j+1} \end{Bmatrix} = \begin{Bmatrix} \mathbf{d}_R^{j} \\ -\mathbf{F}_R^{j} \end{Bmatrix} \tag{2}$$

Substitution of these into Eq. (1) yields

$$\begin{Bmatrix} \mathbf{d}_L^{j} \\ \mathbf{F}_L^{j} \end{Bmatrix} = e^{\mu} \begin{Bmatrix} \mathbf{d}_R^{j} \\ -\mathbf{F}_R^{j} \end{Bmatrix} \tag{3}$$

This final relationship is a result known as periodic structure theory in structural vibro-acoustic analysis [19]. Since this relates the displacements and tractions acting on both edges of a periodic element and the propagation constant is computed from this equation, the wave propagation of a periodic structure can be investigated by considering only a single element.

3. Calculation of propagation constants

If we regard the whole structure of an orthogonally stiffened thin cylindrical shell as an assembly of periodic units, then each unit consists of a bay of the shell, together with half-stiffeners attached at each edge as shown in Fig. 1. The local coordinate system (x,y,z) and displacement components $\mathbf{u}(u,v,w)$ are oriented as shown.

Due to the two-dimensional periodicity of the structure, the displacements, $\mathbf{d}$ and the associated elastic tractions, $\mathbf{t}$ at the left or bottom edge can be related to those at the right or top edge using periodic structure theory, as follows:

$$\begin{Bmatrix} \mathbf{d}_L \\ \mathbf{t}_L \end{Bmatrix} = e^{\mu_x} \begin{Bmatrix} \mathbf{d}_R \\ -\mathbf{t}_R \end{Bmatrix} \tag{4}$$

$$\begin{Bmatrix} \mathbf{d}_B \\ \mathbf{t}_B \end{Bmatrix} = e^{\mu_x} \begin{Bmatrix} \mathbf{d}_T \\ -\mathbf{t}_T \end{Bmatrix} \tag{5}$$

where the structure is assumed to have a constant thickness, and μ_x and μ_y are the propagation constants in the axial and circumferential directions, respectively. It should be noted that the tractions $\mathbf{t}_L$ and $\mathbf{t}_B$ are defined to have the same direction as $\mathbf{t}_R$ and $\mathbf{t}_T$, respectively. For the present study, the assumptions of Mead and Bardell will be employed such that

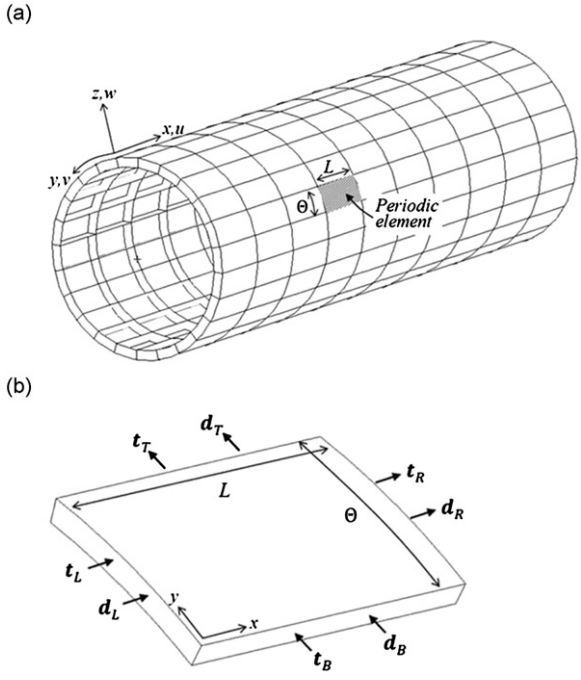

Fig. 1. (a) A thin cylindrical shell with periodic stiffeners; (b) a periodic element with applied tractions and displacements.

the elastic wave is transmitted in the axial direction by using cylindrical symmetry of the shell motions in the circumferential direction and the wave propagation in the circumferential direction is subject to simply-supported boundary conditions at ring frames along axial direction.

3.1. Wave propagation around circumferential direction

In this analysis, a cylinder of radius R and thickness h with 44 axial stringers of length L is considered, as shown in Fig. 2. For a thin circular cylindrical shell made of cross-ply laminates, based on Reissner–Naghdi shell theory [20], the dynamic equations of motion may be written in the form

$$\mathbf{Lu}=\mathbf{0} \tag{6}$$

where $\mathbf{L}$ is a linear differential operator which has the following entries:

$$L_{11}=A_{11}\partial_{xx}+A_{66}\partial_{yy}-I_0\partial_{tt},$$

$$L_{12}=[(A_{12}+A_{66})+(B_{12}+B_{66})/R]\partial_{xy},$$

$$L_{13}=-B_{11}\partial_{xxx}-(B_{12}+2B_{66})\partial_{xyy}+(A_{12}/R)\partial_x,$$

$$L_{22}=(A_{66}+2B_{66}/R+D_{66}/R^2)\partial_{xx}+(A_{22}+2B_{22}/R+D_{22}/R^2)\partial_{yy}-I_0\partial_{tt},$$

$$L_{23}=-[B_{12}+2B_{66})+(D_{12}+2D_{66})/R]\partial_{xxy}-(B_{22}+D_{22}/R)\partial_{yyy}+(A_{22}/R+B_{22}/R^2)\partial_y,$$

$$L_{33}=D_{11}\partial_{xxxx}+2(D_{12}+2D_{66})\partial_{xxyy}+D_{22}\partial_{yyyy}-2[(B_{12}/R)\partial_{xx}+(B_{22}/R)\partial_{yy}]+A_{22}/R^2+I_0\partial_{tt},$$

$$L_{12}=L_{21},\quad L_{13}=L_{31},\quad L_{23}=L_{32}$$

Here A_{ij}, B_{ij}, and D_{ij} $(i,j=1,2,6)$ are extensional, coupling, and bending elastic constants of the shell material. Furthermore, ∂_x, ∂_y, and ∂_t represent partial differentiation with respect to spatial coordinates x and y and time (t). It is noted that, as discussed in [20], the first order shear deformation model becomes more accurate as R/h tends to be smaller values. However, in the present study the cylinder considered has $R/h=500$ for which the shell theory used here is more than adequate.

The displacements, $\mathbf{d}_y$ and the associated tractions, $\mathbf{t}_y^{sh}$ at an edge in line with axial direction of the shell may be written in the forms

$$\mathbf{d}_y=\mathbf{D}_y\mathbf{u} \tag{7}$$

$$\mathbf{t}_y^{sh}=\mathbf{T}_y^{sh}\mathbf{u} \tag{8}$$

where $\mathbf{D}_y$ and $\mathbf{T}_y^{sh}$ are 4 by 3 differential operators with the following non-zero entries:

$$D_{y11}=D_{y22}=D_{y33}=1,\quad D_{y43}=\partial_y,$$

$$T_{y11}^{sh}=A_{66}\partial_y,\quad T_{y12}^{sh}=(A_{66}+B_{66}/R)\partial_x,\quad T_{y13}^{sh}=-2B_{66}\partial_{xy},$$

$$T_{y21}^{sh}=(A_{12}+B_{12}/R)\partial_x,\quad T_{y22}^{sh}=(A_{22}+2B_{22}/R+D_{22}/R^2)\partial_y,$$

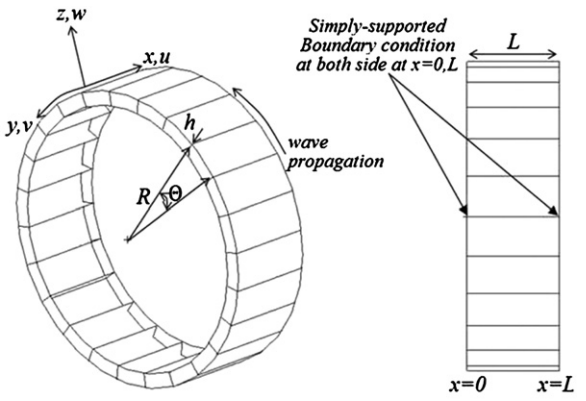

Fig. 2. A periodic unit for circumferential wave analysis.

$$T^{sh}_{y23} = -(B_{12}+D_{12}/R)\partial_{xx} - (B_{22}+D_{22}/R)\partial_{yy} + (A_{22}/R + B_{22}/R^2),$$

$$T^{sh}_{y31} = (B_{12}+2B_{66})\partial_{xy}, \quad T^{sh}_{y32} = 2(B_{66}+D_{66}/R)\partial_{xx} + (B_{22}+D_{22}/R)\partial_{yy},$$

$$T^{sh}_{y33} = -(D_{12}+4D_{66})\partial_{xxy} - D_{22}\partial_{yyy} + (B_{22}/R)\partial_y,$$

$$T^{sh}_{y41} = -B_{12}\partial_x, \quad T^{sh}_{y42} = -(B_{22}+D_{22}/R)\partial_y, \quad T^{sh}_{y43} = D_{12}\partial_{xx} + D_{22}\partial_{yy} - B_{22}/R$$

According to Vlasov's theory of a beam with open cross-section [21], the x, y, and z components of the displacements have the form $u - zw' - yv' - w^*\theta'_x, v - z\theta_x$, and $w + y\theta_x$ where prime indicates the differentiation with respect to x and w^* represents the warping of the cross-section. With the rotary inertia effect and the approximation of angle of twist of the stiffener as $\theta_x = w,y$, the differential equations governing the vibrations of the axial stiffeners may give rise to the following traction component

$$\mathbf{t}^{bm}_y = \mathbf{T}^{bm}_y \mathbf{u} \tag{9}$$

where the entries of $\mathbf{T}^{bm}_y$ are as follows:

$$T^{bm}_{y11} = -EA\partial_{xx} + \rho A\partial_{tt}, \quad T^{bm}_{y12} = -y_H EA\partial_{xxx} + (\rho y_H A\partial_x)\partial_{tt},$$

$$T^{bm}_{y13} = -z_H EA\partial_{xxx} + (\rho z_H A\partial_x)\partial_{tt},$$

$$T^{bm}_{y21} = -T^{bm}_{y12}, \quad T^{bm}_{y22} = EI_{zzH}\partial_{xxxx} + \rho(A - I_{zzH}\partial_{xx})\partial_{tt},$$

$$T^{bm}_{y23} = EI_{yzH}\partial_{xxxx} + \rho(-I_{yzH}\partial_{xx} - z_H A\partial_y)\partial_{tt},$$

$$T^{bm}_{y31} = -T^{bm}_{y13}, \quad T^{bm}_{y32} = EI_{yzH}\partial_{xxxx} + \rho(-I_{yzH}\partial_{xx})\partial_{tt},$$

$$T^{bm}_{y33} = EI_{yyH}\partial_{xxxx} + \rho(A - I_{yyH}\partial_{xx} - y_H A\partial_y)\partial_{tt},$$

$$T^{bm}_{y41} = 0, \quad T^{bm}_{y42} = \rho z_H A\partial_{tt}, \quad T^{bm}_{y43} = EI_\omega\partial_{xxxxy} - GJ\partial_{xxy} + \rho((I_{yyH}+I_{zzH})\partial_y - y_H A)\partial_{tt}$$

where E and G are the elastic moduli of the beam, ρ the mass density, A the cross-sectional area, (y_H, z_H) the location of the beam-shell connecting point, H with respect to the beam centroid, I_{yyH} and I_{zzH} the second moments of area in regard to the point H, and I_ω and J are the torsional coefficients of the beam cross-section.

The above traction terms from both shell and beam are combined to yield the total tractions, $\mathbf{t}_T$ and $\mathbf{t}_B$ at the top and bottom side of the periodic element as

$$\mathbf{t}_T(=\mathbf{T}_T\mathbf{u}_T) = [\mathbf{t}^{sh}_y + \tfrac{1}{2}\mathbf{t}^{bm}_y]_T = [\mathbf{T}^{sh}_y + \tfrac{1}{2}\mathbf{T}^{bm}_y]_T\mathbf{u}_T \tag{10}$$

$$\mathbf{t}_B(=\mathbf{T}_B\mathbf{u}_B) = [-\mathbf{t}^{sh}_y + \tfrac{1}{2}\mathbf{t}^{bm}_y]_B = [-\mathbf{T}^{sh}_y + \tfrac{1}{2}\mathbf{T}^{bm}_y]_B\mathbf{u}_B \tag{11}$$

and the corresponding edge displacements, $\mathbf{d}_T$ and $\mathbf{d}_B$ are easily shown to be

$$\mathbf{d}_T(=\mathbf{D}_T\mathbf{u}_T) = [\mathbf{d}_y]_T = [\mathbf{D}_y]_T\mathbf{u}_T \tag{12}$$

$$\mathbf{d}_B(=\mathbf{D}_B\mathbf{u}_B) = [\mathbf{d}_y]_B = [\mathbf{D}_y]_B\mathbf{u}_B \tag{13}$$

where $[\,\cdot\,]_T$ and $[\,\cdot\,]_B$ stands for value of $[\,\cdot\,]$ evaluated at the top and bottom edges and $\mathbf{u}_T$ and $\mathbf{u}_B$ are the displacements at top and bottom edges, respectively. Note that half the stiffener at a junction interconnects adjacent two shell elements and exerts equal amount of forces on each of them, and the negative sign is introduced to the shell traction component at the bottom edge because $\mathbf{t}^{sh}_y$ was defined to be oriented in the positive coordinates.

These Eqs. (10)–(13), along with the Eqs. (7) and (8) are applicable to arbitrary motion of the shell element with two stiffeners. The specific concern here is with an elastic wave motion which is propagating along circumferential direction while satisfying the simply-supported boundary conditions at two ring locations. Hence, the elastic wave will be taken to have frequency ω and axial wavenumber $k_x = n\pi/l$ $(n = 1,2,3,\ldots)$, so that the shell motion must take the form

$$\mathbf{u} = \begin{Bmatrix} U\cos k_x x \\ V\sin k_x x \\ W\sin k_x x \end{Bmatrix} e^{\lambda y} e^{i\omega t} \tag{14}$$

Substitution of this expression into Eq. (6) yields

$$\mathbf{bU} = \mathbf{0} \tag{15}$$

where the entries of $\mathbf{b}$ may be deduced from those of $\mathbf{L}$ and thus are a function of shell materials and a triad (ω, k, λ). The characteristic equation of $\mathbf{b}$ is a bi-quartic in λ which, for the given ω and k, yields eight eigenvalues λ_m $(m = 1,2,\ldots,8)$ and

eight associated eigenvectors $\mathbf{U}_m=[U_m,V_m,W_m]^{\mathrm{T}}$ from which the shell motion with n fixed may be obtained

$$\mathbf{u}=\sum_{m=1}^{8} C_m \begin{Bmatrix} U_m\cos k_x x \\ V_m \sin k_x x \\ W_m \sin k_x x \end{Bmatrix} e^{\lambda_m y} e^{i\omega t} \tag{16}$$

where C_m is the amplitude of the mth wave and $\mathbf{U}_m$ is normalized such that $W_m=1$. By combining this and Eqs. (10)–(13), Eq. (5) will be written in the form

$$\begin{Bmatrix} \sum_{m=1}^{8} \mathbf{D}_{Bm}\mathbf{U}_m C_m \\ \sum_{m=1}^{8} \mathbf{T}_{Bm}\mathbf{U}_m C_m \end{Bmatrix} = e^{\mu_y} \begin{Bmatrix} \sum_{m=1}^{8} \mathbf{D}_{Tm}\mathbf{U}_m e^{\lambda_m R\Theta} C_m \\ -\sum_{m=1}^{8} \mathbf{T}_{Tm}\mathbf{U}_m e^{\lambda_m R\Theta} C_m \end{Bmatrix} \tag{17}$$

where $\mathbf{D}_{Bm}=\mathbf{D}_B(\lambda_m)$,$\mathbf{D}_{Tm}=\mathbf{D}_T(\lambda_m)$,$\mathbf{T}_{Bm}=\mathbf{T}_B(\lambda_m)$,$\mathbf{T}_{Tm}=\mathbf{T}_T(\lambda_m)$ and $R\Theta$ is the length of the periodic element along circumference. This can be written in more compact form

$$\mathbf{K}_B\mathbf{C}=e^{\mu_y}\mathbf{K}_T\mathbf{C} \tag{18}$$

or

$$\mathbf{K}_T^{-1}\mathbf{K}_B\mathbf{C}=e^{\mu_y}\mathbf{C} \tag{19}$$

where $\mathbf{C}=[C_1,C_2,\ldots C_8]^{\mathrm{T}}$ is the vector form of the wave amplitudes and $\mathbf{K}_B$ and $\mathbf{K}_T$ are 8 by 8 square matrices which are given as follows:

$$\mathbf{K}_T=\begin{bmatrix} \mathbf{D}_{T1}\mathbf{U}_1 e^{\lambda_1 R\Theta} & \mathbf{D}_{T2}\mathbf{U}_2 e^{\lambda_2 R\Theta} & \ldots & \mathbf{D}_{T8}\mathbf{U}_8 e^{\lambda_8 R\Theta} \\ -\mathbf{T}_{T1}\mathbf{U}_1 e^{\lambda_1 R\Theta} & -\mathbf{T}_{T2}\mathbf{U}_2 e^{\lambda_2 R\Theta} & \ldots & -\mathbf{T}_{T8}\mathbf{U}_8 e^{\lambda_8 R\Theta} \end{bmatrix} \tag{20}$$

$$\mathbf{K}_B=\begin{bmatrix} \mathbf{D}_{B1}\mathbf{U}_1 & \mathbf{D}_{B2}\mathbf{U}_2 & \ldots & \mathbf{D}_{B8}\mathbf{U}_8 \\ \mathbf{T}_{B1}\mathbf{U}_1 & \mathbf{T}_{B2}\mathbf{U}_2 & \ldots & \mathbf{T}_{B8}\mathbf{U}_8 \end{bmatrix} \tag{21}$$

Eqs. (18) and (19) are in canonical form for the determination of the eigenvaluese$^{\mu_y}$ from which the complex propagation constants μ_y's or the attenuation constants, real part of μ_y's, are obtained.

3.2. Wave propagation along axial direction

In this analysis, a thin cross-ply cylinder of radius R, thickness h and infinite length in axial direction is considered, as shown in Fig. 3.

Application of Reissner–Naghdi shell theory yields exactly the same dynamic equations of shell motion as Eq. (6), and edge displacements and tractions of the shell are shown to be

$$\mathbf{d}_x=\mathbf{D}_x\mathbf{u} \tag{22}$$

$$\mathbf{t}_x^{sh}=\mathbf{T}_x^{sh}\mathbf{u} \tag{23}$$

where the entries of $\mathbf{D}_x$ and $\mathbf{T}_x^{sh}$ are as follows:

$$D_{x11}=D_{x22}=D_{x33}=1,\quad D_{x43}=\partial_x,$$

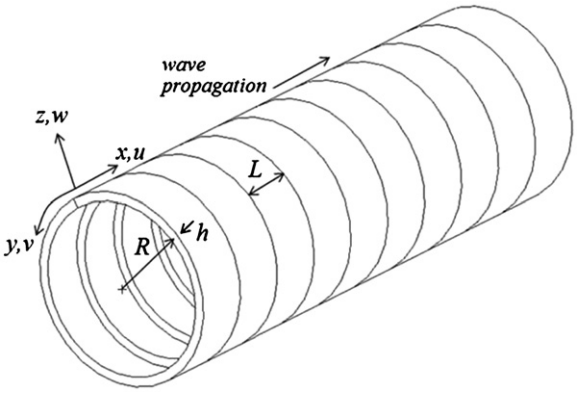

Fig. 3. A periodic unit for axial wave analysis.

$$T^{sh}_{x11}=A_{11}\partial_x,\quad T^{sh}_{x12}=(A_{12}+B_{12}/R)\partial_y,\quad T^{sh}_{x13}=-B_{11}\partial_{xx}-B_{12}\partial_{yy}+A_{12}/R,$$

$$T^{sh}_{x21}=(A_{66}+B_{66}/R)\partial_y,\quad T^{sh}_{x22}=(A_{66}+2B_{66}/R+D_{66}/R^2)\partial_x,$$

$$T^{sh}_{x23}=-2(B_{66}+D_{66}/R)\partial_{xy},$$

$$T^{sh}_{x31}=B_{11}\partial_{xx}+2B_{66}\partial_{yy},\quad T^{sh}_{x32}=(B_{12}+2B_{66}+(D_{12}+2D_{66})/R)\partial_{xy},$$

$$T^{sh}_{x33}=-D_{11}\partial_{xxx}-(D_{12}+4D_{66})\partial_{xyy}+(B_{12}/R)\partial_x,$$

$$T^{sh}_{x41}=-B_{11}\partial_x,\quad T^{sh}_{x42}=-(B_{12}+D_{12}/R)\partial_y,\quad T^{sh}_{x43}=D_{11}\partial_{xx}+D_{12}\partial_{yy}-B_{12}/R$$

Vlasov's beam theory is again employed to obtain the x, y, and z components of the displacements, i.e. $v-xu'-z(w'-v/R)-w*(\theta'_y-u'/R)$, and $w-x\theta_y$ where prime indicates the differentiation with respect to y. This gives

$$\mathbf{t}^{bm}_x=\mathbf{T}^{bm}_x\mathbf{u} \tag{24}$$

where the entries of $\mathbf{T}^{\mathrm{bm}}_x$ are

$$T^{bm}_{x11}=(EI_{zzH}+EI_\omega/R^2)\partial_{yyyy}-(GJ/R^2)\partial_{yy}+\rho(A-I_{zzH}\partial_{yy})\partial_{tt},$$

$$T^{bm}_{x12}=(x_HEA-EI_{xzH}/R)\partial_{yyy}-\rho(x_HA-I_{xzH}/R)\partial_y\partial_{tt},$$

$$T^{bm}_{x13}=(x_HEA/R)\partial_{yy}+EI_{xzH}\partial_{yyyy}-(EI_{zzH}/R+GJ/R)\partial_{xyy}+(EI_\omega/R)\partial_{xyyyy}+\rho(-I_{xzH}\partial_{yy}+z_HA\partial_x)\partial_{tt},$$

$$T^{bm}_{x21}=-T^{bm}_{x12},$$

$$T^{bm}_{x22}=(-EA+2z_HEA/R-EI_{xxH}/R^2)\partial_{yy}+\rho(A-2z_HA/R+I_{xxH}/R^2)\partial_{tt},$$

$$T^{bm}_{x23}=(-EA/R+z_HEA/R^2)\partial_y+(-z_HEA+EI_{xxH}/R)\partial_{yyy}+(x_HEA/R-EI_{xzH}/R^2)\partial_{xy}+\rho(z_HA-I_{xxH}/R)\partial_y\partial_{tt},$$

$$T^{bm}_{x31}=(x_HEA/R)\partial_{yy}+EI_{xzH}\partial_{yyyy}-\rho(I_{xzH}\partial_{yy})\partial_{tt},$$

$$T^{bm}_{x32}=(EA/R-z_HEA/R^2)\partial_y+(z_HEA-EI_{xxH}/R)\partial_{yyy}+\rho(-z_HA+I_{xxH}/R)\partial_y\partial_{tt},$$

$$T^{bm}_{x33}=EA/R^2+(2z_HEA/R)\partial_{yy}+EI_{xxH}\partial_{yyyy}-(x_HEA/R^2+(EI_{xzH}/R)\partial_{yy})\partial_x+\rho(A-I_{xxH}\partial_{yy}-x_HA\partial_x)\partial_{tt},$$

$$T^{bm}_{x41}=(-EI_{zzH}/R-GJ/R)\partial_{yy}+(EI_\omega/R)\partial_{yyyy}+\rho z_HA\partial_{tt},$$

$$T^{bm}_{x42}=(-x_HEA/R+EI_{xzH}/R^2)\partial_y,$$

$$T^{bm}_{x43}=-x_HEA/R^2-(EI_{xzH}/R)\partial_{yy}+(EI_{zzH}/R^2+EI_\omega\partial_{yyyy}-GJ\partial_{yy})\partial_x+\rho(-x_HA+(I_{xxH}+I_{zzH})\partial_x)\partial_{tt}$$

where (x_H,z_H) the location of the beam-shell connecting point in $x-z$ plane with respect to the beam centroid and I_{xxH} and I_{zzH} the second moments of area with in regard to the point, H, of the beam cross-section.

Using the half stiffener method, the resulting edge displacements, $\mathbf{d}_L$ and $\mathbf{d}_R$ and the associated tractions, $\mathbf{t}_L$ and $\mathbf{t}_R$ at the left and right side of the periodic element as

$$\mathbf{d}_L(=\mathbf{D}_L\mathbf{u}_L)=[\mathbf{d}_x]_L=[\mathbf{D}_x]_L\mathbf{u}_L \tag{25}$$

$$\mathbf{d}_R(=\mathbf{D}_R\mathbf{u}_R)=[\mathbf{d}_x]_R=[\mathbf{D}_x]_R\mathbf{u}_R \tag{26}$$

$$\mathbf{t}_L(=\mathbf{T}_L\mathbf{u}_L)=[-\mathbf{t}^{sh}_x+\tfrac{1}{2}\mathbf{t}^{bm}_x]_L=[\mathbf{T}^{sh}_x+\tfrac{1}{2}\mathbf{T}^{bm}_x]_L\mathbf{u}_L \tag{27}$$

$$\mathbf{t}_R(=\mathbf{T}_R\mathbf{u}_R)=[\mathbf{t}^{sh}_x+\tfrac{1}{2}\mathbf{t}^{bm}_x]_R=[\mathbf{T}^{sh}_x+\tfrac{1}{2}\mathbf{T}^{bm}_x]_R\mathbf{u}_R \tag{28}$$

where $\mathbf{u}_L$ and $\mathbf{u}_R$ are the displacements at left and right edges, respectively.

Due to cylindrical symmetry where the radial displacement, w is always in quadrature with the other two components, u and v, the components of the cylinder displacement are described by sinusoidal motion in y and traveling wave motion in x

$$\mathbf{u}=\begin{Bmatrix}U\cos k_y y\\ V\sin k_y y\\ W\cos k_y y\end{Bmatrix}e^{\lambda x}e^{i\omega t} \tag{29}$$

where $k_y=m/R$ ($m=0, 1, 2,\ldots$) is the circumferential wavenumber.

Substituting this into Eq. (6) and solving the resulting characteristic equation as described in the previous section, eight eigenvalues λ_n (n=1, 2,…,8) and eight associated eigenvectors $\mathbf{U}_n=[U_n, V_n, W_n]^T$ may be obtained to yield the following shell motion

$$\mathbf{u}=\sum_{n=1}^{8} C_n \begin{Bmatrix} U_n \cos k_y y \\ V_n \sin k_y y \\ W_n \cos k_y y \end{Bmatrix} e^{\lambda_n x} e^{i\omega t} \tag{30}$$

where C_n is the amplitude of the nth wave and $\mathbf{U}_n$ is normalized such that W_n=1. As before, by combining this and Eqs. (25)–(28), Eq. (4) will be written in the form

$$\mathbf{K}_L\mathbf{C}=e^{\mu_x}\mathbf{K}_R\mathbf{C} \tag{31}$$

or

$$\mathbf{K}_R^{-1}\mathbf{K}_L\mathbf{C}=e^{\mu_x}\mathbf{C} \tag{32}$$

where $\mathbf{C}=[C_1,C_2,\ldots,C_8]^T$ is the vector form of the wave amplitudes and $\mathbf{K}_L$ and $\mathbf{K}_R$ are 8 by 8 square matrices which are given as follows:

$$K_L=\begin{bmatrix} \mathbf{D}_{L1}\mathbf{U}_1 & \mathbf{D}_{L2}\mathbf{U}_2 & \cdots & \mathbf{D}_{L8}\mathbf{U}_8 \\ \mathbf{T}_{L1}\mathbf{U}_1 & \mathbf{T}_{L2}\mathbf{U}_2 & \cdots & \mathbf{T}_{L8}\mathbf{U}_8 \end{bmatrix} \tag{33}$$

$$\mathbf{K}_R=\begin{bmatrix} \mathbf{D}_{R1}\mathbf{U}_1 e^{\lambda_1 l} & \mathbf{D}_{R2}\mathbf{U}_2 e^{\lambda_2 l} & \cdots & \mathbf{D}_{R8}\mathbf{U}_8 e^{\lambda_8 l} \\ -\mathbf{T}_{R1}\mathbf{U}_1 e^{\lambda_1 l} & -\mathbf{T}_{R2}\mathbf{U}_2 e^{\lambda_2 l} & \cdots & -\mathbf{T}_{R8}\mathbf{U}_8 e^{\lambda_8 l} \end{bmatrix} \tag{34}$$

Here, $\mathbf{D}_{Ln}=\mathbf{D}_L(\lambda_n)$, $\mathbf{D}_{Rn}=\mathbf{D}_R(\lambda_n)$, $\mathbf{T}_{Ln}=\mathbf{T}_L(\lambda_n)$, $\mathbf{T}_{Rn}=\mathbf{T}_R(\lambda_n)$, and l is the length of the periodic element along axial direction. This eigenvalue problem can be solved for the complex propagation constants μ_x's or the attenuation constants, real part of μ_x's, as explained in the previous section.

4. Numerical examples

4.1. Flexural wave propagation in axial direction

Propagation constants for axisymmetric mode [22], the case of m=0 in Section 3.2, have been computed over a certain frequency range for a thin cylinder of radius R=0.381 m and ring spacings l=0.135 m with 10 uniformly spaced ring stiffeners. The cylindrical shell itself consists of 4 layers of carbon/epoxy laminates with 0.1905 mm thickness of each lamina and 90/0/0/90 stacking sequence and the circumferential stiffeners are made of aluminum. The detailed material and physical properties of the shell and stiffeners are summarized in Tables 1 and 2. Note that 1 percent structural damping loss factor (η) is used for both shell and stiffeners.

Displacement or velocity ratios between two adjacent bays, i.e. attenuation constants, are calculated for dense FE model of the same dimension using MSC/NASTRAN cyclic symmetry frequency response analysis [23,24] for the comparison with analytic results. An 1.0 degree strip in circumferential direction is considered for finite element analysis and the finite element mesh density is chosen so as to satisfy the condition that at least 10 elements are included in one wavelength of deformation at the maximum frequency of interest which, in this case, is 7079 Hz. An axisymmetric excitation is applied at the far left end of the cylindrical shell (periodic unit 1). Analyses are performed between 3548 and 7079 Hz and these analyzed frequencies are above the ring frequency of the cylindrical shell (around 2973 Hz) such that the axisymmetric mode may be dominant in that frequency range.

The attenuation constant of the flexural wave is first presented in Fig. 4. It can be observed that adding ring stiffeners generates the stop bands to the thin cylinder and, in this particular case, there are four stop bands within the analyzed frequency range.

Table 1
Cross-sectional properties of stiffeners.

Axial stiffeners	
A (m^2)	3.4×10^{-5}
I_{yy} (m^4)	2.0353×10^{-9}
I_{zz} (m^4)	2.8883×10^{-10}
J (m^4)	1.1667×10^{-11}
Ring stiffeners	
A (m^2)	1.2×10^{-5}
I_{xx} (m^4)	1.44×10^{-10}
I_{zz} (m^4)	1.00×10^{-12}
J (m^4)	3.79×10^{-12}

Table 2
Material properties of stiffeners and cylindrical shell.

Aluminum (stiffeners)	
E (Pa)	7×10^{10}
ν	0.3
ρ (kg/m^3)	2700
η	0.01
Carbon/epoxy (cylindrical shell)	
E_1 (Pa)	1.44×10^{11}
E_2 (Pa)	9.38×10^{9}
ν_{12}	0.325
G_{12} (Pa)	5.39×10^{9}
ρ (kg/m^3)	1525
η	0.01

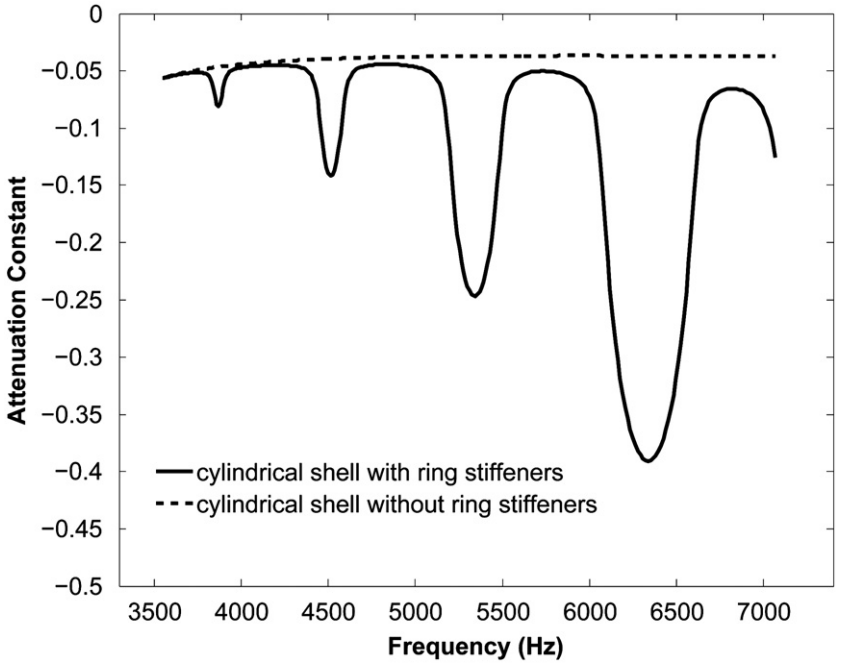

Fig. 4. The flexural wave attenuation constant of axisymmetric mode of the 90/0/0/90 carbon/epoxy laminated cylindrical shell with and without ring stiffeners.

The time averaged kinetic energy stored in the jth periodic unit, KE_j, may be expressed as

$$KE_j = \frac{1}{4}\left(\int_0^L \rho 2\pi Rh|v_j|^2\,\mathrm{d}x\right) \tag{35}$$

where $|v_j|$ is the velocity amplitude of the axisymmetric response and ρ, R and h are, respectively, the mass density, radius and thickness of the cylindrical shell.

Since the velocities at the two adjacent periodic units are related by the propagation constant, i.e., $|v_{j+1}| = \mathrm{e}^{real(\mu)}|v_j|$, the energy ratio ($ER$) between two adjacent units is computed based on the periodic structure theory as

$$ER = \frac{KE_{j+1}}{KE_j} = \frac{\int_0^L \rho 2\pi Rh(\mathrm{e}^{real(\mu)}|v_j|)^2\,\mathrm{d}x}{\int_0^L \rho 2\pi Rh|v_j|^2\,\mathrm{d}x} = (\mathrm{e}^{real(\mu)})^2 \tag{36}$$

Here, the energy ratios of the bending wave between two adjacent bays are computed from the attenuation constants and compared with FEA results as shown in Fig. 5. As shown in the figure, the stop/pass band characteristics due to ring stiffeners are accurately captured and thus the good correlation between finite element and analytical results has been obtained. Notice that, as shown in Figs. 5 and 6, an additional finite element analysis has been performed with twice denser mesh in order to ensure that the FEA solution converged. It should also be noted that, as shown in Fig. 5, there exist some disturbances in all propagation zones of the FEA results due to the finite number of periodic elements. They, however, are too small to affect the validity of the FEA solution to represent the overall pass and stop band characteristics of the periodic

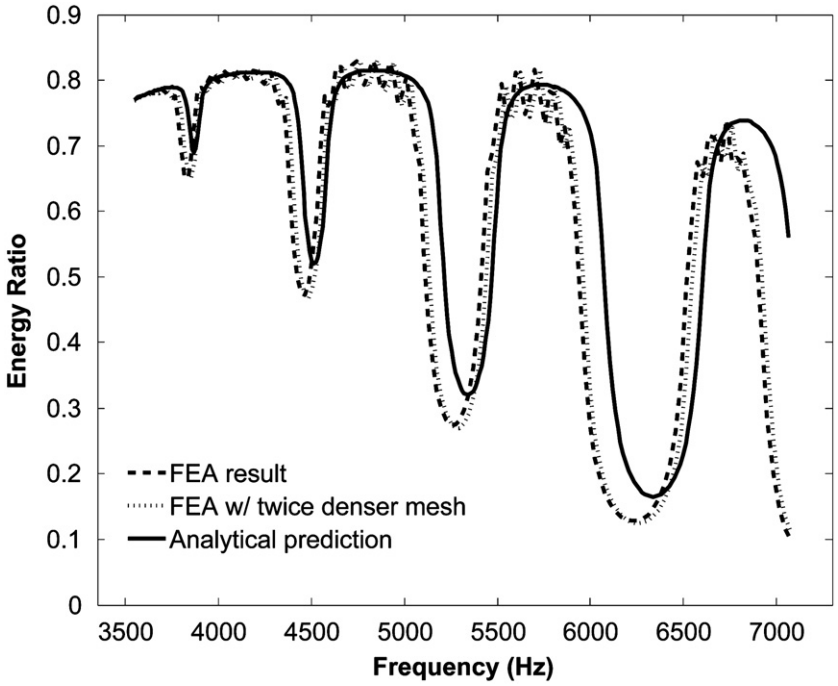

Fig. 5. The energy ratio of the 90/0/0/90 carbon/epoxy laminated cylindrical shell with ring stiffeners subject to axisymmetric excitation.

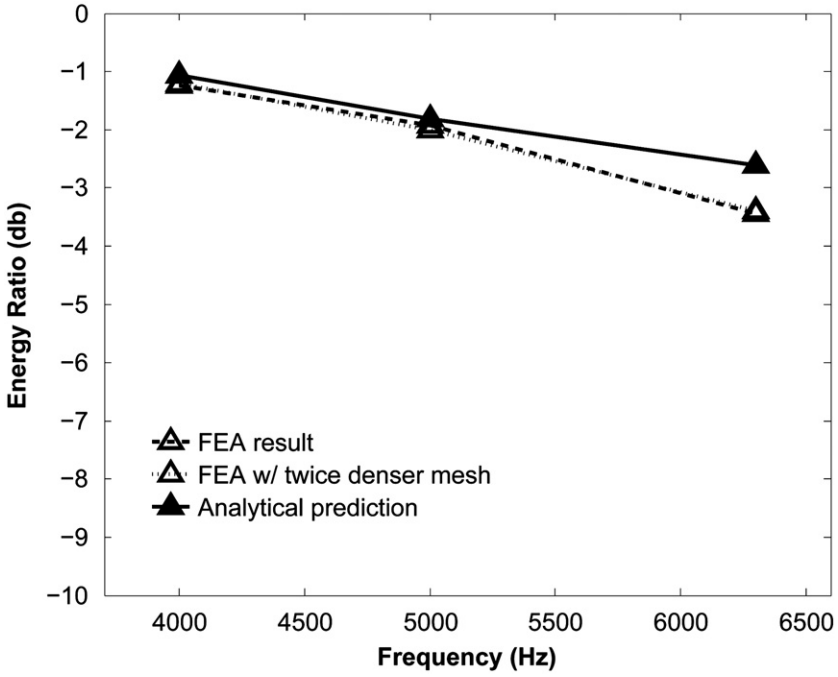

Fig. 6. The frequency averaged energy ratio of the 90/0/0/90 carbon/epoxy laminated cylindrical shell with ring stiffeners under axisymmetric excitation.

structure of interest. Hence, the FEA model can provide a reference solution to which the analytical results can be compared.

In structural acoustics, the frequency and space averaged energy density is of primary importance and the energy level of a receiving periodic unit may be calculated from that of an exciting unit combined with the energy ratio. Thus, the energy ratio is averaged in frequency domain over each 1/3 octave band and is presented in Fig. 6 for the same frequency

range of interest as before. Compared to FEA results, it is shown that the difference between analytical and finite element results is less than 1 dB which is almost negligible in structural acoustics analysis.

4.2. Flexural wave propagation in circumferential direction

Considered in this section is a cylindrical shell of the same dimension as that of the previous section, but in this case with axial stiffeners. The attenuation constants of bending waves propagating in circumferential direction through the 90/0/0/90 carbon/epoxy laminated cylindrical shell with axial stiffeners are presented in Fig. 7 for the first three axial half-wave numbers. As shown in the figure, the flexural waves having one half-wave along axial direction start to propagate at around 1000 Hz and have the first propagation zone from 1000 to 2000 Hz, the second from 2300 to 2750 Hz, the third from 3400 to 3550 Hz, and the fourth 5350 to 5623 Hz. In other words, in the frequency range between 178 and 5623 Hz, flexural waves of $n=1$ have four discrete pass bands between which there are stop bands. Each stop band also has different values of attenuation constants which will determine how much of the flexural energy will be transmitted from a periodic unit to the next one. The flexural waves having two or three half sinusoidal waves in axial direction have pass/stop bands at different frequency zones.

In order to calculate the energy ratio using MSC/NASTRAN, the frequency averaged energy density over each 1/3 octave band is computed over wide frequency range between 200 and 5000 Hz and finally the space averaged energy density in each bay is obtained and used to evaluate the energy ratio between adjacent two periodic units. For the energy ratio computation by the analytical method, the propagation constants corresponding to different half-wave numbers along the length of the longitudinal bay are first calculated and those which undergo a pass band are selected as explained in the previous paragraph, and they are finally used to determine the total response of the structure, i.e. energy ratio between two consecutive bays. Much attention is given to the flexural wave motion of the periodic structure and thus the transverse velocity ratios corresponding to the flexural waves are calculated in this analysis as shown in Fig. 8.

As previously mentioned, the first wave propagation occurs around 1000 Hz at which the given structure has its first natural frequency when there exists one sinusoidal half-wave along longitudinal direction. Between 1000 and 5000 Hz, pass/stop bands exist discretely for each flexural wave. However, since their pass bands are repeated over broad frequency range, if the first pass bands for flexural waves of $n=1,2,3$ are combined, the first pass band for that combination becomes from 1000 to 3000 Hz, the second pass band appears to be 3300–4050 Hz and the third will be from 5350 to 5623 Hz. Moreover, considerably small attenuation constants exist over the stop bands between pass bands. Therefore, the velocity attenuation over one periodic element is shown to be so small over the frequency range between 1000 and 5000 Hz that flexural energy can be transmitted along the axial direction even in this frequency range. This may manifest itself that enormous numbers of vibration modes occur, densely populate the frequency range, and thus all waves having frequencies in this range may propagate with very small attenuation which is mainly due to the structural damping loss factor.

4.3. Effects of material anisotropy and spatial periodicity

In this section, the effects of shell material properties and spatial periodicity on the energy ratio of flexural waves between adjacent periodic elements will be examined based on the analytical approach presented in this paper. Shell bending stiffness and periodic element length are chosen to vary, while other dimensions and material properties are held constant. Throughout the analysis, the principal material directions (1- and 2-axes) are assumed to coincide with the x- and y-axes of the shell coordinate system shown in Figs. 2 and 3.

If flexural waves propagate along the cylinder with the axisymmetric standing wave pattern in circumferential direction, the change in the onset frequency of the axisymmetric mode will result in translation in the frequency axis of the

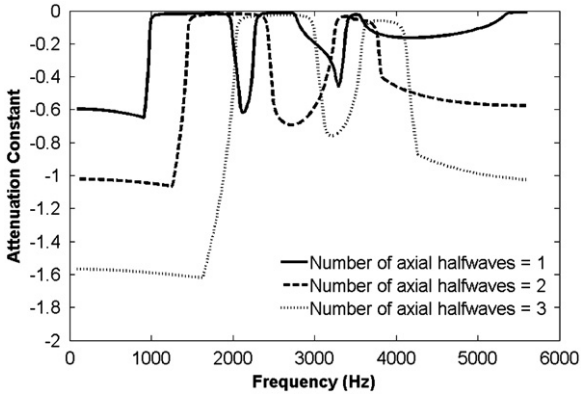

Fig. 7. The flexural wave attenuation constants of the 90/0/0/90 carbon/epoxy laminated cylindrical shell with axial stiffeners with respect to the number of half-waves in axial direction.

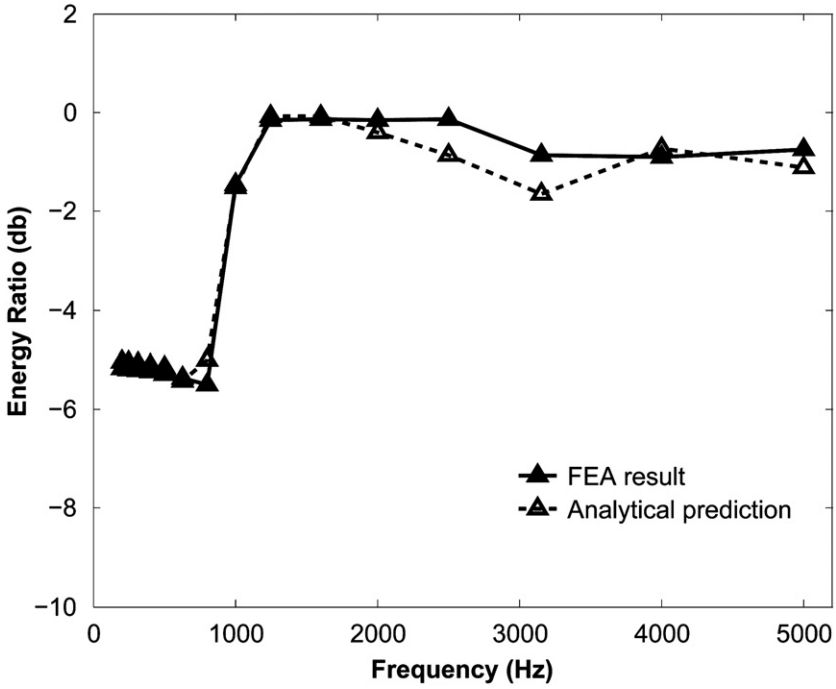

Fig. 8. The frequency averaged flexural energy ratio of the 90/0/0/90 carbon/epoxy laminated cylindrical shell with axial stiffeners.

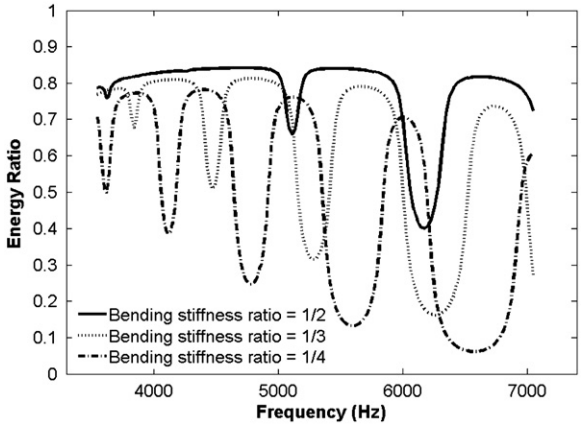

Fig. 9. The effect of bending stiffness ratio, $12(1-\nu^2)D_{11}/Eh^3$, on flexural energy ratio of the laminated cylindrical shell with circumferential stiffeners.

attenuation constant or energy ratio curve. Since axisymmetric modes are initiated by the ring frequency of the cylindrical shell, $\omega_{ring}=\sqrt{A_{22}/\rho hR^2}$, it is apparent that the elastic modulus, A_{22} may cause such shift over the frequency. If A_{22} is held constant, then it is the bending stiffness ratio of shell to ring frame, $12(1-\nu^2)D_{11}/Eh^3$, that needs to be given a special attention among other elastic constants. The attenuation constant curves are shown in Fig. 9 for the three different values of bending stiffness ratios. The number of pass and stop bands is seen to decrease as the bending stiffness ratio increases. This would be attributed to the bandwidth of each propagation zone, $\Delta\omega$, being proportional to D_{11} and thus the increased bandwidth yields fewer propagation zones in the same frequency range of interest. Such relationship between $\Delta\omega$ and D_{11} may be deduced from the Refs. [1,2] in that the lower and upper bounding frequencies of each propagation zone in symmetric periodic systems are proved to coincide with natural frequencies of a single periodic element with free or fixed boundaries. It is also observed in Fig. 9 that the higher bending stiffness ratio enables the more wave energy to propagate with the less reflection. As would be expected, this is due to the fact that the more compliant stiffener tends to lose its ability to block the flexural wave energy of shell across stiffeners and vice versa.

The axial length of each periodic element, l, has also influence on the flexural wave propagation along the cylinder. In order to show the effect of the length, l, with respect to the circumferential length of the same bay, $R\Theta$, the length ratio,

$l/R\Theta$, is considered here with $R\Theta$ being fixed. Fig. 10 shows that the larger length yields the more frequent pass/stop bands. Since the difference between the bounding frequencies, $\Delta\omega$, is inversely proportional to l, the increased length ratio may result in more frequent repetition of propagation and attenuation zones. The lower propagated energy level for a higher length ratio may need the explanation detailed in what follows. As an elastic wave propagates, it may experience attenuation arising from either the structural damping or the structural discontinuity. The amount of wave amplitude attenuation due to the structural damping is proportional to the distance over which a wave propagates. Moreover, according to periodic structure theory, the wave amplitude will be attenuated across a circumferential stiffener by $e^{\mathrm{Real}(\mu)l}$. Both of the wave attenuation mechanism give rise to the wave energy loss proportional to the length, l. Hence, the longer length results in the smaller energy being propagated over one periodic length.

In the case of the flexural wave propagating along the circumference, the first propagation zone begins (and the first attenuation zone ends) at the first natural frequency of the stiffened cylinder subject to a sinusoidal half-wave in the longitudinal direction (This phenomenon has been shown in Section 4.2 and the detailed theoretical proof can also be found in the literature [1,2]). Therefore, the changes in bending stiffness in the circumferential direction, D_{22} and/or the number of axial stringers may result in the change in the frequency. Such effect has been shown in Fig. 8 as the steep increase in energy ratio across 1000 Hz, the first natural frequency of the stiffened cylinder considered in Section 4.2. For the evaluation of wave propagation characteristics in higher frequencies, however, the frequency range of 1413–7079 Hz is used and thereby the first attenuation zone is not shown in the following figures.

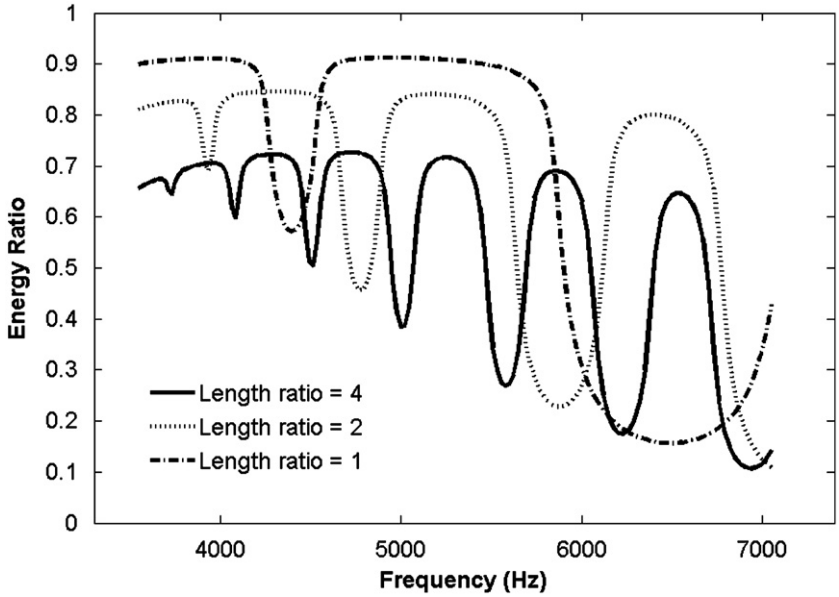

Fig. 10. The effect of length ratio, $l/R\Theta$, on flexural energy ratio of the laminated cylindrical shell with circumferential stiffeners.

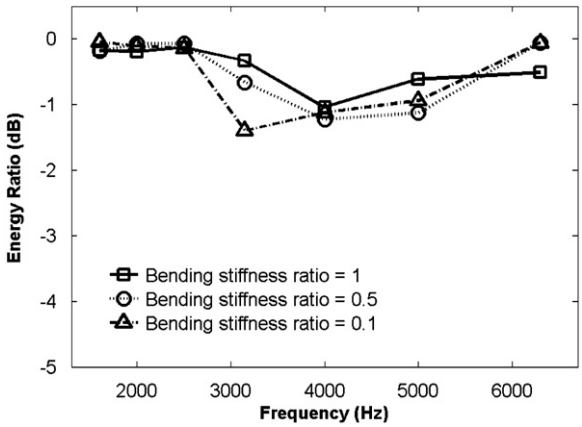

Fig. 11. The effect of bending stiffness ratio, $12(1-\nu^2)D_{22}/Eh^3$, on flexural energy ratio of the laminated cylindrical shell with axial stiffeners.

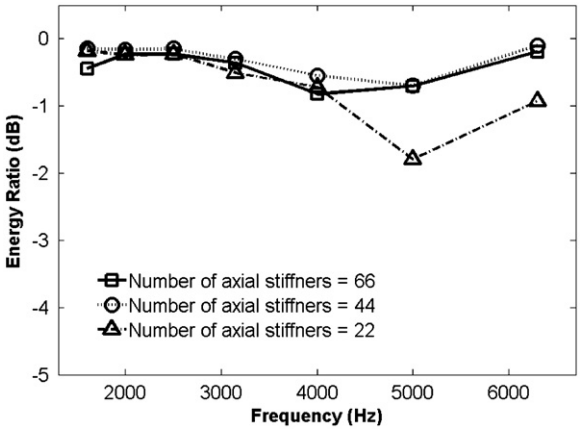

Fig. 12. The effect of the number of axial stiffeners on flexural energy ratio of the laminated cylindrical shell with axial stiffeners.

If the bending stiffness ratio, $12(1-\nu^2)D_{22}/Eh^3$, and the number of axial stiffeners are chosen to vary, they are expected to affect the pass/stop band characteristics of the flexural waves with different sinusoidal half-waves. For instance, the location of each pass or stop band may change depending on the value of bending stiffness ratio and the number of axial stiffeners. However, when several half-waves are combined to yield space- and frequency-averaged energy ratios, the changes in the location of pass and stop bands are likely to be smeared out to give almost same energy ratios in lower frequency regions as shown, respectively, in Fig. 11 (up to 2500 Hz) and Fig. 12 (up to 4000 Hz). In higher frequency range, however, it is still observed that the greater the bending stiffness ratio is and the more the axial stiffeners are used, the more energy may transfer from one periodic element to another. Since the number of axial stiffeners can be expressed as $2\pi/\Theta$ and thus is inversely proportional to the circumferential length of each periodic element, $R\Theta$, the flexural wave energy propagation with respect to the bending stiffness ratio and the number of axial stiffeners can be explained in the same manner as for the case of flexural wave propagating in axial direction.

5. Conclusion

The periodic structure theory is utilized for calculating propagation constants of a composite cylindrical shell stiffened periodically by metallic circumferential stiffeners and axial stringers, which is of particular significance in vibro-acoustic analysis of periodic structures. Since the two-dimensional periodic structures do not normally exhibit a single pass or stop band at a particular frequency as is the case for one-dimensional periodic structures, the propagation constants corresponding to several different circumferential modes or/and several different half-wave numbers along the length of the cylinder should be calculated in order to identify the pass band characteristics when a circumferentially and axially stiffened cylinder is analyzed. The propagation constants corresponding to these circumferential modes (for ring stiffeners) or half-wave numbers (for axial stringers) are combined to determine the energy ratios of this kind of structure. The validation through some vibration analyses in the previous section demonstrates that the analytical method shown in this paper captures well the periodic characteristics for a thin composite cylinder with the axial stringers and ring stiffeners.

Based on the current analytical approach, the effects of shell material properties and spatial periodicity on the wave propagation characteristics have been evaluated in terms of flexural wave energy transferred from one periodic element to another. Among others, the bending stiffness and the length of a single periodic element in axial and circumferential directions were chosen to vary. It has been shown that the more flexural wave energy can transmit in the axial direction as the bending stiffness ratio of the shell to the ring stiffeners increases and the length of one periodic element decreases. The flexural energy propagation in circumferential direction tends to be triggered by the first natural frequency so that the shell material properties and the number of axial stiffeners can be used as control variables for the wave energy propagation in higher frequency region as well as the onset frequency of the first wave propagation. These parametric study reveals that both the material anisotropy (the different material properties in axial and circumferential direction) and spatial periodicity (length of each periodic element in both directions) can be properly exploited to control the amount of energy attenuation in propagating elastic waves by the means of the proposed method of combining periodic structure theory and laminate theory.

Acknowledgments

The present research in this paper was supported by National Aeronautics and Space Administration under Contract Number NNXO7ADO6A.

References

[1] G. Sen Gupta, Natural flexural waves and the normal modes of periodically-supported beams and plates, *Journal of Sound and Vibration* 13 (1970) 89–101.
[2] D.J. Mead, Wave propagation and natural modes in periodic systems: I. Mono-coupled systems, *Journal of Sound and Vibration* 40 (1975) 1–18.
[3] D.J. Mead, Wave propagation and natural modes in periodic systems: I. Multi-coupled systems, with and without damping, *Journal of Sound and Vibration* 40 (1975) 19–39.
[4] D.J. Mead, Wave propagation in continuous periodic structures: research contributions from Southampton, *Journal of Sound and Vibration* 190 (1996) 495–524.
[5] D.J. Mead, N.S. Bardell, Free vibration of a thin cylindrical shell with discrete axial stiffeners, *Journal of Sound and Vibration* 111 (1986) 229–250.
[6] D.J. Mead, N.S. Bardell, Free vibration of a thin cylindrical shell with periodic circumferential stiffeners, *Journal of Sound and Vibration* 115 (1987) 499–520.
[7] N.S. Bardell, D.J. Mead, Free vibration of an orthogonally stiffened cylindrical shell, part I: discrete line simple supports, *Journal of Sound and Vibration* 134 (1989) 29–54.
[8] N.S. Bardell, D.J. Mead, Free vibration of an orthogonally stiffened cylindrical shell, part II: discrete general stiffeners, *Journal of Sound and Vibration* 134 (1989) 55–72.
[9] C.H. Hodges, J. Power, J. Woodhouse, The low frequency vibration of a ribbed cylinder, part 1: theory, *Journal of Sound and Vibration* 101 (1985) 219–235.
[10] M.B. Xu, X.M. Zhang, W.H. Zhang, Space-harmonic analysis of input power flow in a periodically stiffened shell filled with fluid, *Journal of Sound and Vibration* 222 (1999) 531–546.
[11] J.H. Lee, J. Kim, Sound transmission through periodically stiffened cylindrical shells, *Journal of Sound and Vibration* 251 (2002) 431–456.
[12] J. Yan, T.Y. Li, T.G. Liu, J.X. Liu, Characteristics of the vibrational power flow propagation in a submerged periodic ring-stiffened cylindrical shell, *Applied Acoustics* 67 (2006) 550–569.
[13] A.M. Wang, N. Vlahopoulos, R.D. Buehrle, J. Klos, Energy finite element analysis of the NASA aluminum testbed cylinder, *SAE Noise and Vibration Conference* Paper Number 2005-01-2372, 2005.
[14] N. Vlahopoulos, Energy finite element analysis for computing the high frequency vibration of the aluminum testbed cylinder and correlating the results to test data, *NASA/CR-2005-213760*, 2005.
[15] W. Zhang, N. Vlahopoulos, K. Wu, An energy finite element formulation for high frequency vibration analysis of externally fluid-loaded cylindrical shells with periodic circumferential stiffeners subjected to axi-symmetric excitation, *Journal of Sound and Vibration* 282 (2005) 679–700.
[16] X. Zhao, K.M. Liew, T.Y. Ng, Vibrations of rotating cross-ply laminated circular cylindrical shells with stringer and ring stiffeners, *International Journal of Solids and Structures* 39 (2002) 529–545.
[17] R.T. Wang, Z.X. Lin, Vibration analysis of ring-stiffened cross-ply laminated cylindrical shells, *Journal of Sound and Vibration* 295 (2006) 964–987.
[18] L. Brillouin, *Wave Propagation in Periodic Structures*, McGraw-Hill, New York, 1946.
[19] L. Cremer, M. Heckl, E.E. Ungar, *Structure-borne Sound*, second ed., Springer-Verlag, Berlin, 1988.
[20] M.S. Qatu, *Vibration of Laminated Shells and Plates*, Elsevier Academic Press, New York, 2004.
[21] T.H.G. Megson, *Aircraft Structures for Engineering Students*, third ed., Butterworth Heinemann, New York, 1999.
[22] A. Leissa, *Vibration of Shells*, Acoustical Society of America, New York, 1993.
[23] MSC.NASTRAN 2004, *Advanced Dynamic Analysis User's Guide*, MSC.Software Corporation.
[24] MSC.NASTRAN 2004, *Linear Static Analysis User's Guide*, MSC.Software Corporation.